JOURNAL OF MAGNETIC RESONANCE **130,** 335–340 (1998)
ARTICLE NO. MN971321

HSQC-based Methyl Group Selection via Gradients in Multidimensional NMR Spectroscopy of Proteins

Tammo Diercks, Manfred Schwaiger, and Horst Kessler

Institut für Organische Chemie und Biochemie, Technische Universität München, Lichtenbergstraße 4, 85747 Garching, Germany

E-mail: kessler@artus.org.chemie.tu-muenchen.de

Received June 25, 1997; revised November 6, 1997

A quadruple-quantum filtered HSQC (QQF-HSQC) for the selection of methyl groups which minimizes the line-broadening effects of proton homonuclear couplings is presented. The scheme uses gradients for *n*-quantum coherence selection and solvent suppression. In contrast to the heteronuclear quadruple-quantum coherence (HQQC) approach, the QQF-HSQC allows for long constant-time (CT) evolution, making use of the generally favorable relaxation properties of methyl groups. The increase in resolution and concomitant gain in sensitivity is discussed in theory and demonstrated in practice on the 14-kDa human nonpancreatic synovial phospholipase A2 (hnps-PLA2). The constant-time version is particularly useful for obtaining high-resolution spectra as demonstrated on hnps-PLA2. The applicability of the CT-QQF-HSQC module in multidimensional experiments is demonstrated using a 3D CT NOESY-QQF-HSQC spectrum of the 31-kDa homodimeric IIAMan domain of the mannose transporter of *E. coli*.

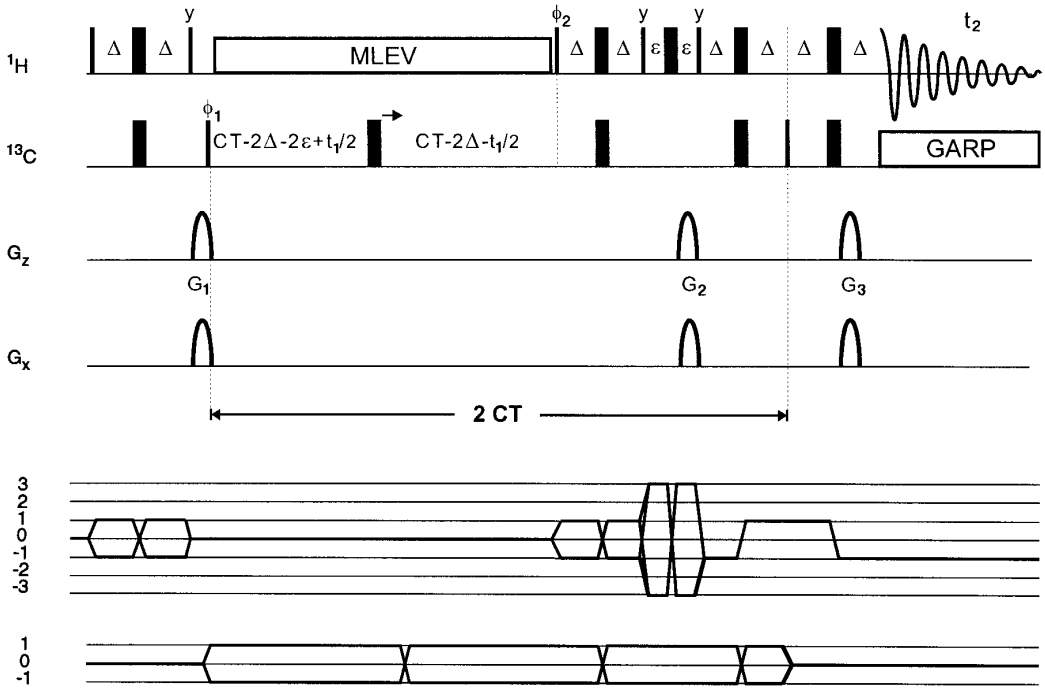

FIG. 1. Pulse sequence of the constant-time quadruple-quantum filtered HSQC (CT-QQF-HSQC) experiment with the relevant coherence-transfer pathways. Narrow and wide bars indicate 90° and 180° pulses, respectively. All pulses were applied with phase x if not otherwise indicated. The phase cycles used in this experiment were $\phi_1 = x, -x$; $\phi_2 = 2x, 2(-x)$ and $\phi_{rec} = x, 2(-x), x$. In the constant-time period the arrow indicates the direction in which the pulse is shifted as t_1 is incremented; the delays were set as follows: $\Delta = 2$ ms, CT = 12.3 ms. Proton decoupling was achieved by a MLEV16 expansion of 180° pulses. Frequency discrimination in F_1 was achieved using the echo–antiecho procedure. Pulsed field gradients of relative amplitudes $G_1 = 20$, $G_2 = -20$, $G_3 = 65$ for p-selection and $G_1 = 20$, $G_2 = -20$, $G_3 = 55$ for the n-selection were applied for a duration of 1.0 ms, followed by 0.2 ms recovery delays. All gradient pulses were applied at an angle of 54.7° relative to the z coordinate according to the relation $G_x = \sqrt{2} \cdot G_z$.

1090-7807/98 $25.00

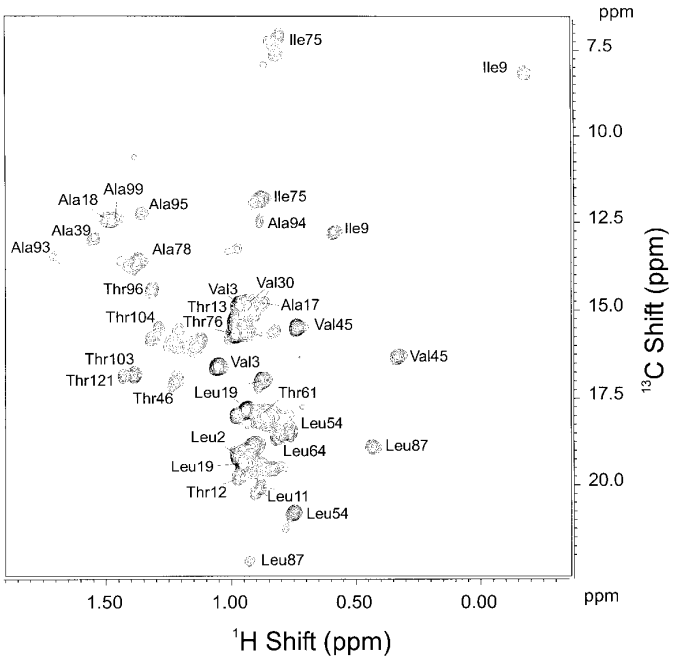

FIG. 2. CT-QQF-HSQC spectrum of 0.6 mM hnps-PLA_2 at 600 MHz and 310 K recorded using the sequence in Fig. 1. Delays and gradients were set as given in the legend to Fig. 1. Carrier frequencies were set to 14.5 ppm in F_1 and to 1.0 ppm in F_2. A total of 512 data points was acquired with a spectral width of 2400 Hz, corresponding to an acquisition time of 106.5 ms. In the indirect dimension, 88 data points were collected for a spectral width of 2700 Hz. The spectrum was sampled with 16 scans per transient and a 1.0 s recycle delay, resulting in an experiment duration of 35 min. Linear prediction using 24 coefficients was applied in F_1, generating 40 additional data points. Data were zero filled to 1024 × 256 points, and a squared cosine-bell window function in both dimensions was applied.

Methyl group selection is a way to improve resolution in H,C correlation spectroscopy (*1–6*) by limiting the spectral width. It has become a common strategy in deriving valuable distance constraints from the methyl groups of hydrophobic residues in proteins. Typically a DEPT (*7*) module is applied to create heteronuclear quadruple-quantum coherence (HQQC) (*1, 5*), and coherence selection is achieved using either the phase cycling method (*1–5, 8, 9*) or the more recent gradient selection scheme (*6, 9–11*). The main disadvantage of the HQQC experiment is homonuclear coupling between the methyl protons and other protons. These passive couplings lead to phase distortions, additional line broadening, and invariably a sensitivity loss proportional to the proton multiplicity of the multiquantum coherence (*12*). It is therefore not possible to acquire high-resolution spectra, which require long indirect acquisition times t_1, with homogeneous phases using the HQQC approach. Here we present an HSQC experiment with a quadruple-quantum filter (the QQF-HSQC) and gradient selection designed to minimize the detrimental effects of homonuclear proton couplings, and thus allow for high-resolution spectra with pure phases.

The method is discussed for its constant time (*13, 14*) version as shown in Fig. 1. After an initial INEPT step, carbon single-quantum coherence evolves during time t_1. Carbon magnetization remains transverse throughout the constant time 2*CT which is chosen to maximize $\cos(\pi * {}^1J_{CC} * 2CT) * \exp(-2CT/T_2)$ for $CT > 0$. Here, T_2 stands for the effective carbon spin–spin relaxation time and ${}^1J_{CC} = 35$ Hz is the single-bond carbon–carbon coupling. The carbon coherence is kept antiphase with respect to one coupled proton by means of continuous proton decoupling. A 90°_x proton pulse then creates proton–carbon zero- and double-quantum coherence $2C_yH_y$. During the following delay of $2*\Delta = 2*1/4{}^1J_{HC}$, carbon spins evolve antiphase to all other attached protons resulting in the term $2^nC_{xy}H_yH_z^{n-1}$, where n is the proton multiplicity for the carbon considered. A subsequent 90°_y proton pulse creates maximum-quantum coherence $2^nC_{xy}H_yH_x^{n-1}$

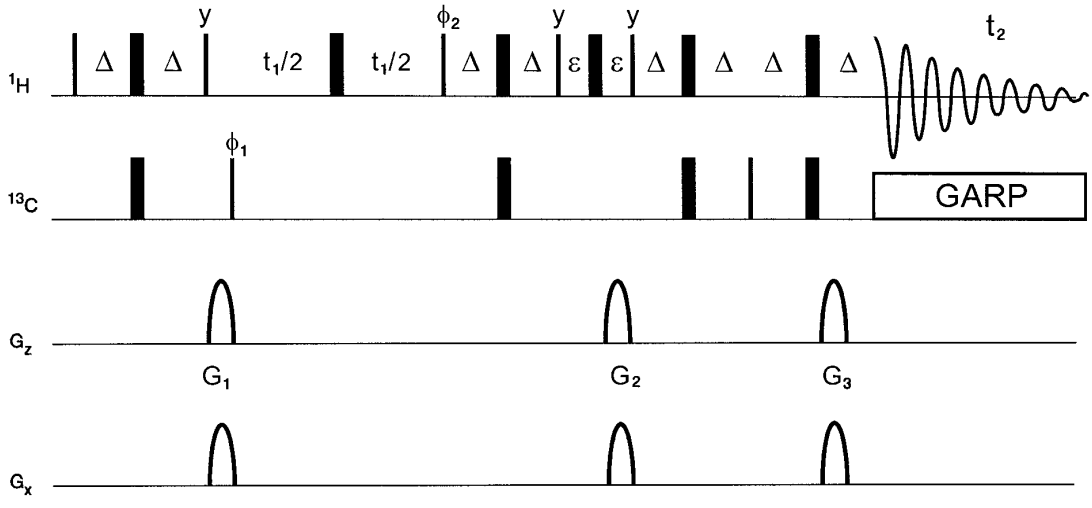

FIG. 3. Pulse sequence of the QQF-HSQC with a variable time delay during the evolution of ^{13}C magnetization. All parameters, pulse phases, and gradient strengths are identical to those given in Fig. 1.

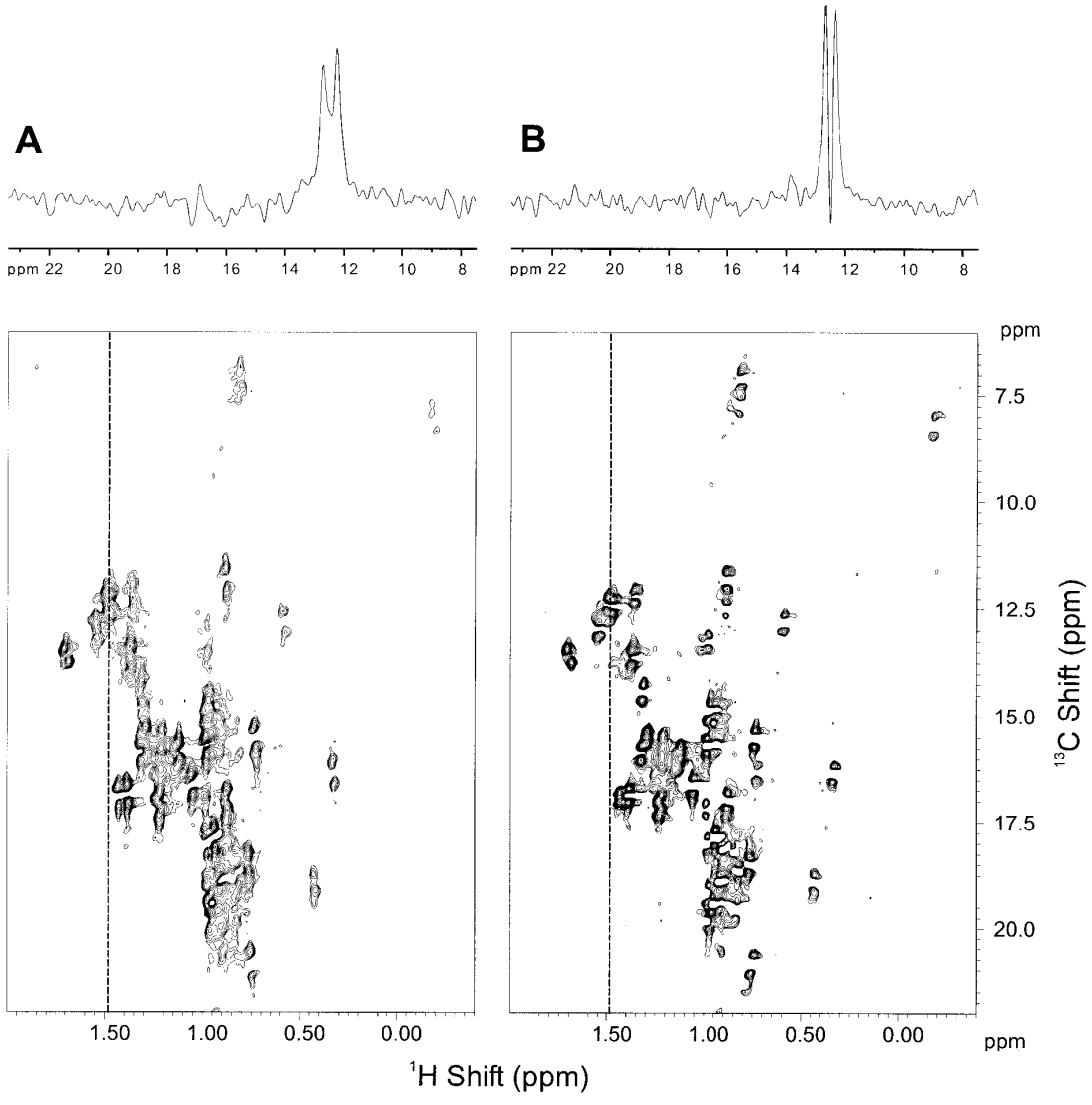

FIG. 4. Comparison of the HQQC (A) versus the QQF-HSQC (B) spectrum of hnps-PLA$_2$. Experimental conditions were the same as those for the constant-time experiment shown in Fig. 2, except that 256 data points were collected in F_1. Data were zero filled to 1024 × 512 points, and a squared cosine-bell window function in both dimensions was applied. Both spectra are plotted with identical contour levels. Superimposed columns of the Ala18 methyl group at 1.48 ppm demonstrate the intensity gain of the QQF-HSQC versus the HQQC. As explained in the text, the apparent doublet splitting caused by the $^1J_{CC}$ coupling of 35 Hz is increased as a result of dephasing due to the evolution of the coupling. Note the much larger apparent doublet splitting of the HQQC caused by the inherently larger linewidth of this experiment.

which is required for the multiplicity selection. The hetero n-quantum coherence persists throughout the labeling time 2ε required for coherence selection during the dephasing gradient G_2. This labeling time can easily be included in the carbon shift evolution time, t_1, by appropriately moving the preceding t_1-shifted carbon refocusing pulse. Thus, no resolution is lost due to the implementation of selection gradients as $t_{1\max} = 2CT - 4\Delta$ is independent of ε. After the phase labeling of hetero n-quantum coherence, another 90°_y proton pulse reverts the H_x^{n-1} components to $2^nC_{xy}H_yH_z^{n-1}$. During another period $2*\Delta = 2*1/4^1J_{HC}$, $n-1$ J_{HC} couplings refocus to yield $2C_yH_y$, which is then converted to $2C_zH_y$ by the final 90°_x carbon pulse. Subsequently, the proton antiphase coherence refocuses to proton in-phase coherence and is detected after a final rephasing gradient G_3.

Coherence selection is achieved via gradients using the phase-sensitive echo–antiecho method. This selection scheme, which has already been applied to HQQC experiments (*6*, *9–11*), is superior to the alternative selection scheme via phase cycling as it avoids subtraction artifacts and efficiently suppresses undesired coherences (*15*). To select for hetero n-quantum coherences, it is only necessary to adjust the gradient G_3 according to the general selection equation

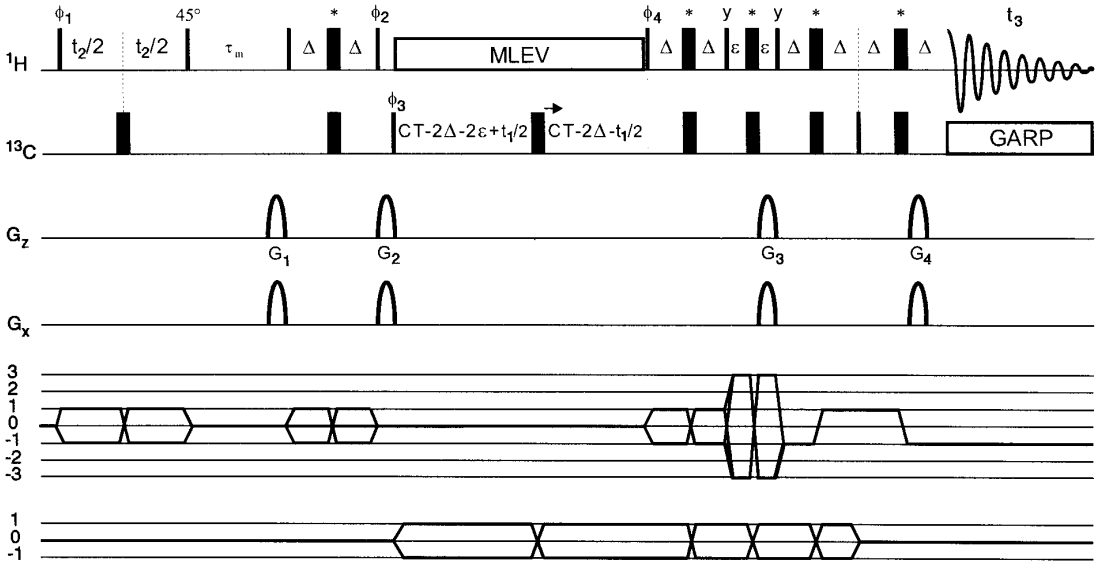

FIG. 5. Pulse sequence of the 3D CT NOESY-QQF-HSQC experiment. All parameters and details for the constant time QQF-HSQC module are as given in the legend to Fig. 1. Proton 180° pulses marked with an asterisk (*) were applied as $90^\circ_x - 180^\circ_y - 90^\circ_x$ composite pulses. An additional *z*-spoil gradient of strength $G_1 = 20$ was inserted at the end of the NOE mixing period τ_m. The phase cycles used in this experiment were $\phi_1 = 4(x), 4(-x)$; $\phi_2 = 8(y), 8(-y)$; $\phi_3 = x, -x$; $\phi_4 = 2x, 2(-x)$; and $\phi_{rec} = x, 2(-x), x, -x, 2(x), 2(-x), 2(x), -x, x, 2(-x), x$. Quadrature detection in t_2 was achieved by incrementing phase ϕ_1 in the States–TPPI manner. The proton 90° pulse at the beginning of the NOE mixing time τ_m was applied with a phase of 45° to ensure uniform water saturation for odd and even numbered t_2 transients.

$$G_3 = -G_2 \frac{n\gamma_H \pm \gamma_C}{\gamma_H}, \qquad [1]$$

where the sum stands for the echo and the difference stands for the antiecho path. The selection equation [1] directly follows from a consideration of the product operators in effect during gradients G_2 and G_3. These are given, respectively, as

$$8H_yC_yH_x^{n-1}\sin^n(\pi\,{}^1J_{HC}2\Delta)\cos(\pi\,{}^1J_{CC}[2CT - 2\Delta]) \qquad [2]$$

$$H_x\sin^{2n}(\pi\,{}^1J_{HC}2\Delta)\cos(\pi\,{}^1J_{CC}2CT). \qquad [3]$$

To further optimize the solvent suppression, we implemented a *z*-spoil gradient G_1 and employed ''magic angle'' gradients throughout G_2 and G_3 by setting $G_x = \sqrt{2}G_z$ to prevent the rephasing of intermolecular multiple-quantum coherences of water molecules (*16–19*). This scheme allowed us to increase the receiver gain from 4K to 64K (maximum receiver gain supported by the spectrometer).

While gradients offer superior selectivity, they have the disadvantage of allowing only the detection of half of the total magnetization due to the restriction to either the *p*- or the *n*-type transfer pathway. This problem can be minimized with a sensitivity enhancement scheme (*20*). However, this has not been applied here as the expected gain for a CH_3 group (less than 10% in practice) is only minimal (*21*).

An application of the CT-QQF-HSQC experiment is shown in Fig. 2 for a 0.6 mM sample of the 14-kDa $^{13}C/^{15}N$-labeled human non-pancreatic synovial phospholipase A_2 (hnps-PLA_2) dissolved in 95% H_2O and 5% D_2O. The spectrum was recorded at 300K using 16 transients and a total of 88 complex data points in the indirect dimension, resulting in an FID resolution of 30.7 Hz in the F_1 dimension. The total experiment time was 35 minutes. Carrier frequencies were set to 1.1 ppm (^1H) and 17.5 ppm (^{13}C). The delays were set to CT = 12.3 ms and Δ = 2 ms. The relaxation delay was set to 1.2 s. One-millisecond sine-shaped gradient pulses and 200-μs recovery delays were used, resulting in ε = 1.2 ms. As can be seen from Fig. 2, the spectrum retains pure absorptive phases and high intensities even for long constant time delays of $2CT \approx 1/{}^1J_{CC}$. In contrast, a comparable high-resolution CT-HQQC would not be practical: phase inhomogeneity caused by the evolution of homonuclear proton couplings would require *magnitude* calculation and would invariably result in greatly reduced intensities due to the overlap of positive and negative signal components.

Recently, Shaw *et al.* (*22*) presented a constant-time HQQC experiment using the shared incrementation time approach (*23, 24*). It has a maximum incrementable time $t_{1max} = 4\Delta$ (where $\Delta_{min} = 1/4\,{}^1J_{HC}$). This short evolution time allows one to obtain largely homogeneous phases even in the presence of homonuclear proton couplings, yet limits the FID resolution in the indirect dimension. If fast relaxation

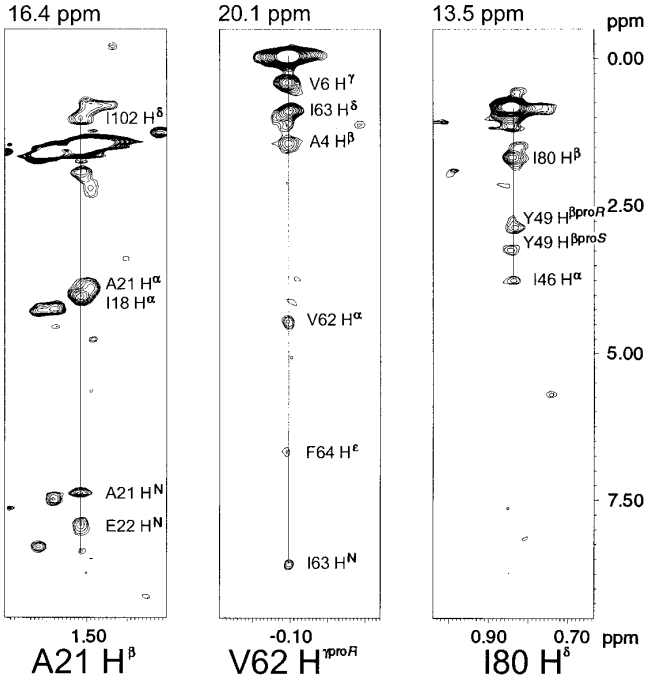

FIG. 6. ^{1}H,^{1}H strips taken at the methyl ^{13}C shifts of Ala21, Val62$^{pro\text{-}R}$, and Ile80$^{\delta}$, from the 3D CT NOESY-QQF-HSQC spectrum of a 1.4 mM sample of the IIA^{Man} domain of the mannose transporter of *E. coli*, a homodimer of 31 kDa total molecular weight. The NOE mixing period τ_m was 80 ms and the constant time delay 2*CT was set to 24.6 ms. All other delays, gradient durations, and gradient strengths were set as given in the legends to Figs. 1 and 5. Carrier frequencies were set to 19.5 ppm in F_1 and to 5.5 ppm in F_2 and F_3. A total of 1024 data points was acquired with a spectral width of 7300 Hz, corresponding to an acquisition time of 70 ms. In the F_2 dimension, 108 data points were collected with the same spectral width. In F_1, 48 data points were collected with a spectral width of 3165 Hz. The spectrum was sampled with 32 scans per transient and a 1.2-s recycle delay, resulting in an experiment duration of 66 h. Linear prediction using 24 coefficients was applied in F_2, generating 52 additional data points. Data were zero filled to 1024 × 256 × 64 points and a squared cosine-bell window function was applied to all dimensions. A zero-order phase correction of −45° was required in F_2 since the proton read pulse after the t_2 evolution time has a phase of 45° (see legend to Fig. 5). A fifth-order polynomial baseline correction was applied in the F_3 dimension over the range from 3.5 to 0 ppm.

is the critical aspect, this experiment should perform better than the CT-QQF-HSQC for which t_{1max} = 2CT-4Δ. However, methyl groups usually have comparatively long T_2 relaxation times due to their fast rotation and may thus permit the use of longer constant time delays. Also, much intensity is gained using the CT-QQF-HSQC due to the absence of attenuation caused by homonuclear proton couplings.

The gain resulting from the absence of homonuclear proton couplings can easily be calculated. Each transverse proton component in the magnetization term concurrently evolves homonuclear couplings. Only the respective in-phase components will eventually be refocused to observable single-quantum coherence. The transfer efficiency in the presence of such passive couplings can thus be calculated as

$$\prod_i \prod_j \cos^{m_i}(\pi J_{HH,j}\tau_i), \qquad [4]$$

where i runs over all segments of duration τ with m_i transverse proton components and j runs over all relevant homonuclear couplings to the protons considered, $J_{HH,j}$. As an approximation, the product $\prod_j J_{HH,j}$ may be substituted by the dominant vicinal $^{3}J_{HH,j}$ coupling. In the case of only one vicinal proton, the corresponding transfer efficiency for both the constant time (Fig. 1) and the nonconstant time version (Fig. 3) of the QQF-HSQC then amounts to

$$\cos^4(2\pi^3 J_{HH}\Delta)\cos^n(2\pi^3 J_{HH}\varepsilon), \qquad [5]$$

with n being the proton multiplicity. For the HQQC experiment, the transfer efficiency is

$$\cos^2(4\pi^3 J_{HH}\Delta)\cos^n(\pi^3 J_{HH}[t_1 + 2\varepsilon]). \qquad [6]$$

In the constant time version of the HQQC experiment, the variable delay $[t_1 + 2\varepsilon]$ in Eq. [6] must be replaced by the constant-time delay 2CT.

Considering exclusively the attenuation due to homonuclear proton coupling (Eq. [5] and Eq. [6]), the QQF-HSQC has an inherently higher sensitivity than the HQQC. However, the faster relaxation of carbon single-quantum versus carbon multiple-quantum coherence (*25*) and accumulated errors in the lengths of the additional pulses in the QQF-HSQC may cause the HQQC to be slightly more sensitive, although only for very short t_1 times. Particular care should therefore be taken in exactly determining the required pulse widths.

As a verification of the expected gain, we have recorded spectra of hnps-PLA$_2$ using the HQQC (Figs. 4A) and the QQF-HSQC (Figs. 4B) experiments, both in the nonconstant time versions. Experimental conditions were the same as those for the constant time CT-QQF-HSQC experiment shown in Fig. 2. Superimposed columns of corresponding signals show that the signal-to-noise ratio is, on average, 40% better for the QQF-HSQC experiment.

The observed signal splittings due to the $^{1}J_{CC}$ coupling are considerably larger than the theoretical value of 35 Hz, with an average of 50 Hz for the QQF-HSQC and 70 Hz for the HQQC. These increases can easily be accounted for by the fact that the $^{1}J_{CC}$ coupling has already evolved for the substantial period of $4\Delta + 2\varepsilon \approx 10$ ms at the beginning of the t_1 sampling period. The resulting phase distortion amounts up to ±60° (opposite signs for both lines of the doublet) and can clearly be seen from the depicted columns. Assuming a linewidth of 30 Hz, the apparent $^{1}J_{CC}$ coupling would increase to the observed 50 Hz in the QQF-HSQC. As mentioned above, the linewidth in the HQQC is larger due to the passive proton couplings. Hence, the apparent $^{1}J_{CC}$ coupling increases even further.

The QQF-HSQC may easily be implemented into three-dimensional experiments. Figure 5 shows the implementation of the scheme into a constant-time 3D NOESY-QQF-HSQC. Figure 6 shows strips taken from the 80-ms 3D CT NOESY-QQF-HSQC of a 1.4 mM aqueous solution of the IIA^{Man} domain of the mannose transporter of *E. coli*, a homodimer of 31 kDa total molecular weight (*26*). As can be seen from the depicted strips, the spectrum reveals important interresidual long-range contacts.

In this Communication we have presented a new HSQC experiment with a gradient-selected heteronuclear quadruple-quantum filter as an alternative to the common DEPT-based HQQC experiments. In contrast to the HQQC, the QQF-HSQC experiment largely removes co-evolution of homonuclear proton couplings and thus permits high-resolution spectra with pure phases. The resulting gain in intensity has been calculated and verified on a representative spectrum. The scheme performs well both as a constant-time 2D QQF-HSQC and as a constant-time 3D NOESY-QQF-HSQC experiment. Its advantages are most prominent if high-resolution spectra are desired.

ACKNOWLEDGMENTS

This work was supported by the Deutsche Foschungsgemeinschaft and the Fonds der chemischen Industrie. We also thank Dr. Gerd Gemmecker for helpful discussions.

REFERENCES

1. H. Kessler, P. Schmieder, and M. Kurz, *J. Magn. Reson.* **85,** 400 (1989).
2. H. Kessler, P. Schmieder, and H. Oschkinat, *J. Am. Chem. Soc.* **112,** 8599 (1990).
3. P. Schmieder, H. Kessler, and H. Oschkinat, *Angew. Chem. (Int. Ed. Engl.)* **29,** 546 (1990).
4. H. Kessler and P. Schmieder, *Biopolymers* **31,** 621 (1991).
5. H. Kessler, P. Schmieder, M. Köck, and M. Reggelin, *J. Magn. Reson.* **91,** 375 (1991).
6. M. Liu, R. D. Farrant, J. K. Nicholson, and J. C. Lindon, *J. Magn. Reson. A* **112,** 208 (1995).
7. D. M. Doddrell, D. T. Pegg, and M. R. Bendell, *J. Magn. Reson.* **48,** 323 (1982).
8. J. M. Schmidt and H. Rüterjans, *J. Am. Chem. Soc.* **112,** 1279 (1990).
9. M. Liu, R. D. Farrant, J. K. Nicholson, and J. C. Lindon, *J. Magn. Reson. B* **106,** 270 (1995).
10. L. Mitschang, H. Ponstingl, D. Grindrod, and H. Oschkinat, *J. Chem. Phys.* **102,** 3089 (1995).
11. T. Parella, F. Sanchez-Ferrando, and A. Virgili, *J. Magn. Reson. A* **117,** 78 (1995).
12. K. V. Schenker and W. von Philipsborn, *J. Magn. Reson.* **61,** 294 (1985).
13. A. Bax, A. F. Mehlkopf, and J. Smidt, *J. Magn. Reson.* **35,** 167 (1979).
14. M. G. Munowitz, R. G. Griffin, G. Bodenhausen, and T. H. Huang, *J. Am. Chem. Soc.* **103,** 2529 (1981).
15. J. Keeler, R. T. Clowes, A. L. Davis, and E. D. Laue, *in* ''Methods in Enzymology'' (N. J. Oppenhaimer and T. L. James, Eds.), Vol. 239, p. 145, Academic Press, San Diego (1994).
16. L. Mattiello, W. S. Warren, L. Mueller, and B. T. Farmer II, *J. Am. Chem. Soc.* **118,** 3253 (1996).
17. P. C. M. van Zijl, M. O. Johnson, S. Mori, and R. E. Hurd, *J. Magn. Reson. A* **113,** 265 (1995).
18. R. E. Hurd, *J. Magn. Reson.* **87,** 422 (1990).
19. A. L. Davis, E. D. Laue, J. Keeler, D. Moskau, and J. Lohmann, *J. Magn. Reson.* **94,** 637 (1991).
20. A. G. Palmer III, John Cavanagh, P. E. Wright, and M. Rance, *J. Magn. Reson.* **93,** 151 (1991).
21. J. Schleucher, M. Schwendinger, M. Sattler, P. Schmidt, O. Schedletzky, S. J. Glaser, O. W. Sørensen, and C. Griesinger, *J. Biomol. NMR* **4,** 301 (1994).
22. G. L. Shaw, T. Müller, H. R. Mott, H. Oschkinat, I. D. Campbell, and L. Mitschang, *J. Magn. Reson.* **124,** 479 (1997).
23. T. M. Logan, E. T. Olejniczak, R. X. Xu, and S. W. Fesik, *J. Biomol. NMR* **3,** 225 (1993).
24. S. Grzesiek, J. Anglister, and A. Bax, *J. Magn. Reson. B* **101,** 114 (1993).
25. A. Bax, M. Ikura, L. E. Kay, D. A. Torchia, and R. Tschudin, *J. Magn. Reson.* **86,** 217 (1990).
26. S. Seip, J. Balbach, S. Behrens, H. Kessler, K. Flükiger, R. de Meyer, and B. Erni, *Biochemistry* **33,** 7174 (1994).